https://doi.org/10.5194/acp-2020-507
Preprint. Discussion started: 10 August 2020
© Author(s) 2020. CC BY 4.0 License.

Atmospheric Chemistry and Physics Discussions

Measurement Report:

Size distributions of inorganic and organic components in particulate matter from a megacity in northern China: dependence upon seasons and pollution levels

Yingze Tian[*,a], Yinchang Feng[a], Yongli Liang[a], Yixuan Li[a], Qianqian Xue[a], Zongbo Shi[b], Jingsha Xu[b], Roy M. Harrison[*,b†]

[a] State Environmental Protection Key Laboratory of Urban Ambient Air Particulate Matter Pollution Prevention and Control, College of Environmental Science and Engineering, Nankai University, Tianjin, 300071, China

[b] School of Geography Earth and Environmental Science, University of Birmingham, Birmingham, B15 2TT, UK

Correspondence to: Roy M. Harrison (r.m.harrison@bham.ac.uk), Yingze Tian (tianyingze@hotmail.com)

[†]Also at: Department of Environmental Sciences / Center of Excellence in Environmental Studies, King Abdulaziz University, PO Box 80203, Jeddah, 21589, Saudi Arabia

https://doi.org/10.5194/acp-2020-507
Preprint. Discussion started: 10 August 2020
© Author(s) 2020. CC BY 4.0 License.

Atmospheric Chemistry and Physics Discussions

Abstract:

Size distributions of inorganic and organic components in particulate matter (PM) provide critical information on its sources, fate and pollution processes. Here, ions, elements, carbon fractions, n-alkanes, polycyclic aromatic hydrocarbons (PAHs), hopanes and steranes in size-resolved (9 stages) PM were analyzed during one year in a typical northern Chinese industrial megacity (Tianjin). We found that the concentrations of organic carbon fraction OC3, NO_3^- (or SO_4^{2-}) and the sum of crustal elements were the highest in the pseudo-ultrafine (<0.43 μm), fine (0.41-2.1 μm) and coarse (>2.1 μm) modes, respectively. The diagnostic ratios of organic components consistently suggest that the traffic influence was stronger during summer and coal combustion during winter. Nitrate and high molecular weight PAHs were concentrated in the fine mode during winter, while nitrate and low molecular weight PAHs showed bimodal distributions especially during summer due to repartitioning. Long-chain *n*-alkanes showed a peak in the coarse mode during spring and summer, indicating a relatively stronger vegetation source and resuspended dust. Furthermore, we found a major difference in the size distribution of aerosol components during heavy pollution episodes (PM_{10}>233 μg m^{-3}) in different seasons: in spring, OC fractions, 4- and 5-ring PAHs, hopanes and C18-C33 n-alkanes were enhanced at 1.1-3.3 μm, implying that they may arise from local combustion sources which emit relatively large particles; in summer PM mass, SO_4^{2-}, NH_4^+, Al, and C26-C33 *n*-alkanes were enhanced mainly in the coarse mode, peaking at 5.8-9.0 μm, indicating a large contribution from resuspended dust or heterogeneous reactions on dusts; in the winter and autumn, NO_3^-

https://doi.org/10.5194/acp-2020-507
Preprint. Discussion started: 10 August 2020
© Author(s) 2020. CC BY 4.0 License.

Atmospheric Chemistry and Physics Discussions

was significantly enhanced followed by SO_4^{2-}, NH_4^+, OC and EC with their peaks shifting from 0.43-0.65 μm to 0.65-2.1 μm, indicating strong atmospheric processing. These results reveal that the size distributions of inorganic and organic aerosol components are dependent on the seasons and pollution levels as a result of the differing sources and physicochemical processes.

1 Introduction

Atmospheric particulate matter (PM) negatively affects human health and visibility, influences global climate change and nutrient cycles within ecosystems (Burnett et al., 2014; Wang et al., 2014; Zhang et al., 2017). Properties and effects of PM depend on their chemical composition and particle sizes (Seinfeld and Pandis, 1998; Kanakidou et al., 2005; Kompalli et al., 2020). PM cover a wide range of sizes from a few nanometers to several hundreds of micrometers, and is composed of a complex mixture of inorganic substances (such as water-soluble ions, elements, and elemental carbon) and hundreds of organic compounds. Several studies have shown that the size distribution of chemical components can provide evidence for examining the sources and formation pathways (Guo et al., 2014; Yao et al., 2018; Hilario et al., 2020).

Non-polar organic compounds in PM, such as n-alkanes, polycyclic aromatic hydrocarbons (PAHs), hopanes and steranes, can provide specific information to identify PM sources (Oros and Simoneit, 2000; Wang et al., 2009; Han et al., 2018). PAHs are mainly emitted from anthropogenic activities, such as biomass burning, coal

https://doi.org/10.5194/acp-2020-507
Preprint. Discussion started: 10 August 2020
© Author(s) 2020. CC BY 4.0 License.

Atmospheric Chemistry and Physics Discussions

combustion, oil combustion and industrial processes (Mastral et al., 1996; Liu et al., 2012). Hopanes and steranes are abundant in coal, crude oils and the lubricant oil fraction, and are often found in traffic exhaust and coal combustion emissions (Oros and Simoneit, 2000). n-Alkanes can arise from both natural and anthropogenic activities, including abrasion products from vegetation leaf surfaces (characterized by the predominance of > C29 odd n-alkanes) and fossil fuel combustion (Han et al., 2018). Although these organic compounds are assumed to be relatively stable and nonreactive (Feng et al., 2006; Ma et al., 2011), they can undergo complex physical and chemical changes, like photochemical oxidation and gas-particle partitioning (Robinson et al., 2006; Han et al., 2018). The size distributions of the organic compounds are strongly associated with their sources, physical behavior and chemical reactions. Several studies on size distributions of PM chemical components have been conducted for ions, elements, and carbon fractions (Dillner et al., 2006; Huang et al., 2016; Tian et al., 2016; Hilario et al., 2020), and for some organic compounds (Wang et al., 2009; Han et al., 2018; Xu et al., 2020). These studies indicated that the size distributions of the inorganic or organic components may vary with season and degree of pollution, so characterizing the variations is valuable for understanding their sources and fate. However, the combined analysis of seasonal variations of inorganic and organic components based on whole year sampling has rarely been conducted.

Severe atmospheric PM pollution has been a recurring problem affecting developing countries (Cheng et al., 2016; Zou et al., 2017). As one of the world's fastest-developing economic zones, the Jing-Jin-Ji economic circle in China has experienced severe and

https://doi.org/10.5194/acp-2020-507
Preprint. Discussion started: 10 August 2020
© Author(s) 2020. CC BY 4.0 License.

Atmospheric Chemistry and Physics Discussions

long-lasting haze episodes (Guo et al., 2014; Long et al., 2019). The "Jin" is Tianjin, a megacity with a population of 15.6 million. With gross industrial production ranking third among all Chinese provinces (TMSB, 2017), Tianjin is a typical industrial city. Various anthropogenic emissions, including industrial emissions, coal combustion, vehicle exhaust and resuspended dust, significantly contribute in this region. Additionally, the chemical and physical characteristics of PM are complex during different seasons. High reactivity due to relative humidity (RH) during winter has been reported (Cheng et al., 2016), and strong dust and sea salt emissions during spring and summer can increase the surfaces needed for heterogeneous reactions. The factors that influence heavy pollution in different seasons remain unclear due to their complexity (Cheng et al., 2016; Yao et al., 2018). The variation of size-resolved inorganic and organic chemical component size distributions during periods of heavy pollution in different seasons can throw light on the mechanisms of PM pollution (Tian et al., 2016; Xu et al., 2020).

In this study, we conducted a comprehensive study of water-soluble ions, elements, carbon fractions, n-alkanes, PAHs, hopanes and steranes in size-resolved PM (9 stages) samples collected from May 2018 to April 2019 in Tianjin, China. The goal of this study is to (1) determine size-resolved chemical composition, including inorganic and organic components, (2) characterize seasonal variations of size distribution of inorganic and organic markers, (3) explore the mechanisms of PM pollution during different seasons through investigating the changes in composition as well as size distribution. The results of this work will help researchers better understand the sources, physical process

https://doi.org/10.5194/acp-2020-507
Preprint. Discussion started: 10 August 2020
© Author(s) 2020. CC BY 4.0 License.

Atmospheric Chemistry and Physics Discussions

and chemical mechanisms of PM pollution during different seasons, which is crucial for evaluating the effects of PM on human health, visibility and regional radiative forcing, and for developing control strategies.

2 Methods and materials

2.1 Study area and sampling

Tianjin is located at 116°43'E~118°04'E, 38°34'N~40°15'N, in the northern part of the North China Plain. It covers an area of 11947 km^2, near the Capital of China (Beijing) and bordering on the Bohai Sea. The population is 15.6 million. As a municipality directly under the Central Government and one of the first coastal open cities, Tianjin is a typical industrial city and a major manufacturing base for some industrial products, whose gross industrial production ranks third among all Chinese provinces (TMSB, 2017). The industries include petroleum and chemical, modern metallurgy, aerospace, automobile and equipment manufacturing, amongst others. More than 20 million tons of coal is consumed by industries and residential heating every year. The civil motor vehicle fleet in Tianjin is about 2.8 million. The Tianjin Port is the largest comprehensive port in northern China and a major port for foreign trade.

The PM samples were collected by an Andersen air sampler (Andersen Series E-0162, USA) with 9-stage size ranges of >9.0, 9.0-5.8, 5.8-4.7, 4.7-3.3, 3.3-2.1, 2.1-1.1, 1.1-0.65, 0.65-0.43, and < 0.43 μm. Quartz-fibre filters (81 mm in diameter) were used. The sampling period was from May 2018 to April 2019, involving spring (May in 2018, and March and April in 2019), summer (June and August in 2018), autumn (1

https://doi.org/10.5194/acp-2020-507
Preprint. Discussion started: 10 August 2020
© Author(s) 2020. CC BY 4.0 License.

Atmospheric Chemistry and Physics Discussions

September to 15 November 2018) and winter (15 November 2018 to 15 March 2019, when coal was consumed for residential heating). The sampling was conducted for 47 h during spring and summer, and for 23 h during autumn and winter, and was stopped during rainy days. Overall, 153 sets of successfully size-resolved samples (total 1377 fraction samples) were obtained. Additionally, the $PM_{2.5}$ and PM_{10} mass concentrations were continuously monitored by a Beta Particulate Monitor (BPM-200, Focused Photonics, China) at the sampling site. The correlation plots between $PM_{2.1}$ and PM_{10} mass concentrations sampled by the Andersen sampler (PM-measured) vs corresponding means of continuous $PM_{2.5}$ and PM_{10} concentrations monitored by the BPM (PM-monitored) were showed in Figure S1. High correlations (0.86 and 0.82) were observed.

To explore the mechanisms of heavy pollution, the heavy pollution was defined as the days with PM_{10} concentrations higher than the 3rd quartile of all the samples, which was 233 μg m^{-3}.

2.2 Chemical analysis of ions, elements and carbon fractions

In this work, 7 ions, 17 elements, 7 carbon fractions, 18 PAHs, 2 cholestane, 7 hopane and 24 n-alkanes were analyzed on each size range. For ion analyses, including Na^+, K^+, Ca^{2+}, NH_4^+, Cl^-, NO_3^- and SO_4^{2-}, one eighth of each quartz filter was cut. The sample was placed in a centrifuge tube which had been ultrasonically cleaned and dried, before addition of 8 ml of distilled deionized water, then placed in an ultrasonic bath for 20 minutes. The sonicated centrifuge tube was refrigerated for 24 hours. The clear

https://doi.org/10.5194/acp-2020-507
Preprint. Discussion started: 10 August 2020
© Author(s) 2020. CC BY 4.0 License.

Atmospheric Chemistry and Physics Discussions

liquid in the middle of the centrifuge tube was withdrawn with a needle tube, filtered through two 0.2 μm filters, and injected into the sample bottle. Lastly the extraction liquid was analyzed to determine the cation and anion concentrations with a Thermo ICS900 Ion Chromatograph (Thermo Electron). For the elemental analysis, 17 elements (Al, Ca, Ti, K, Mg, Na, V, Fe, Cu, Zn, Mn, Pb, As, Cd, Co, Cr, Ni) were analyzed by inductively coupled plasma-mass spectrometry (ICP-AES) (IRIS Intrepid II, Thermo Electron). We cut one eighth of each quartz filter into portions and extracted elements into acid solution (HNO_3: HCl: H_2O_2 = 1: 3: 1) using a microwave digester (PyNN Corporation). Carbon fractions were analyzed by a thermal/optical carbon aerosol analyzer (DRI 2001A, Atmoslytic Inc.), which gives OC1, OC2, OC3, OC4, OP, EC1, EC2, EC3 fractions. The instrument is based on heating and releasing organic carbon and elemental carbon at different temperatures, and uses He-Ne laser to allow quantification of the pyrolytic (OP) fraction. The IMPROVE-A thermal/optical reflectance (TOR) protocol was used (Chow et al., 1993) with 140°, 280°, 480°, 580°, 740°, and 840°C to divide the carbon fractions.

2.3 Chemical analysis of organic components

Organic compounds in half of total sample filters were analyzed by gas chromatography-mass spectrometry (GC-MS). The full names and corresponding abbreviations of organic compounds were summarized in Table 1.

Table 1

For extraction, the filters were cut into portions and put into tubes. Then 10 ml of

https://doi.org/10.5194/acp-2020-507
Preprint. Discussion started: 10 August 2020
© Author(s) 2020. CC BY 4.0 License.

Atmospheric Chemistry and Physics Discussions

dichloromethane (DCM) and 10 ml of n-hexane (1:1, v:v) were added into each tube which was then put in an ultrasonic bath at 30 ℃ for 15 minutes. The solution was filtered with a silica column to clean up the extract. The silica column was eluted with 20 ml of DCM/hexane (1:1) and the extract was collected. After reduction to less than 5 ml (about 2 or 3 ml) by rotary evaporator, the extract was solvent-exchanged to n-hexane. Finally, the volume was reduced to 1 ml. Calibrations of PAHs, hopanes, steranes and n-alkanes were used to test chromatographic conditions before analysing samples. A DB-5MS fused-silica capillary column (30 m × 0.25 mm, 0.25 mm film thickness, Agilent Technology) was used in the GC separation procedure. The carrier gas was pure helium (purity of 99.99% or more) at a constant flow rate of 1.0 mL min^{-1}. For PAHs, hopanes and steranes, inlet and transfer line temperatures were set to 230 ℃ and 280 ℃ respectively. EI mode was used and the ionization energy level was 70eV. For n-alkane analysis, inlet and transfer line temperatures were set to 300 ℃.

2.4 Quality assurance and quality control (QA/QC)

Throughout the whole process, much attention was given to ensure quality assurance and control. All samples were collected by one instrument and analyzed by the same methods. When it rained, we stopped the sampling campaign. The air flow rate was corrected by a flowmeter before each sampling period. Before use, the quartz filters were baked in an oven at 400-500 ℃ to eliminate any organic matter that may exist on the filters. All the filters were equilibrated at room temperature for 48 h in desiccators before weighting. Each filter was weighted by a sensitive microbalance with balance

https://doi.org/10.5194/acp-2020-507
Preprint. Discussion started: 10 August 2020
© Author(s) 2020. CC BY 4.0 License.

Atmospheric Chemistry and Physics Discussions

195 sensitivity ±0.010 mg. The quartz filters were kept in aluminum foil bags before and
196 after sampling until analysis, and stored at −4 °C. The samples were analyzed within
197 30 days.

198 Field and laboratory blanks were measured to correct the corresponding data.
199 Standard reference materials were analyzed with the same procedure every day and the
200 recovered values for all the target components showed low relative standard deviations.
201 Additionally,, the first sample of every ten samples was re-examined with the precision
202 found to be within 10%. The recoveries were 79-106% for elements, and 96-110% for
203 ions. For carbon fractions, a system stability test (three-peak detection) is required
204 before and after detecting samples and the relative standard deviation should not exceed
205 5%. For organic compounds, all extractions were conducted two times so that the
206 samples were extracted adequately, with the tubes sealed by foil and ice added to the
207 ultrasonic bath. The internal standards (naphthalene-d8, acenaphthene-d10,
208 phenanthrene-d10, chrysene-d12, and perylene-d12; hexamethylbenzene; n-
209 tetracosane-d50) were used for the samples to qualify actual volumes of the target
210 compounds present. The calibration curves were strongly linear. The recoveries of most
211 organic compounds ranged from 70%-130%, except for Nap, Any, Ana, C10, and C11
212 with recoveries below 50%.
213
214 **2.5 Diagnostic ratios**
215 Diagnostic ratios were used to identify the sources. The Ant/(Ant+Phe) ratio for
216 PAHs is used to differentiate petroleum origins or pyrogenic sources, and IPY/BghiP

https://doi.org/10.5194/acp-2020-507
Preprint. Discussion started: 10 August 2020
© Author(s) 2020. CC BY 4.0 License.

Atmospheric Chemistry and Physics Discussions

is for different fossil fuels. The ratio of C29αβ/C30αβ for hopane can also be used to judge fossil fuels. The homohopane index C34[S/(S+R)] can distinguish fuel maturity, which is defined as:

$$C34[S/(S+R)] = \frac{\mathrm{C34\alpha\beta S}}{\mathrm{C34\alpha\beta S+C34\alpha\beta R}} \quad (1)$$

For n-alkanes, the carbon preference index (CPI) can reflect the comparison between natural and anthropogenic contributions, which is defined as the ratio of the total concentration of odd n-alkanes to that of even n-alkanes:

$$\mathrm{CPI} = \frac{\sum_{i=5}^{16} C_{2i+1}}{\sum_{i=5}^{16} C_{2i}} \quad (2)$$

where i is the carbon number. Due to that plant wax n-alkanes show strong odd carbon number predominance, biogenic n-alkanes should have CPI values greater than unity, whereas anthropogenic n-alkanes should have CPI values close to unity (Han et al., 2018).

Contributions from natural wax n-alkanes (WNA%) and petrogenic n-alkanes (PNA%) can directly present the origins. The negative value of $[C_i - (C_{i-1} + C_{i+1})/2]$ should be replaced by zero.

$$\mathrm{WNA\%} = \frac{\sum_{i=10}^{32}[C_i - (C_{i-1}+C_{i+1})/2}{\sum_{n=10}^{33} C_n} \quad (3)$$

$$\mathrm{PNA\%} = 100\% - \mathrm{WNA\%} \quad (4)$$

3 Results and discussion

3.1 Size distribution of PM mass concentrations

Figure 1 describes the size distribution of PM mass concentrations in spring, summer, autumn and winter. The average concentrations of PM were the greatest during winter,

https://doi.org/10.5194/acp-2020-507
Preprint. Discussion started: 10 August 2020
© Author(s) 2020. CC BY 4.0 License.

Atmospheric Chemistry and Physics Discussions

239 followed by spring, autumn and summer at most sizes. The size distribution of the PM
240 mass concentrations was bimodal, with one peak at 0.43-0.65 μm (fine mode) and the
241 other at 4.7-5.8 μm (coarse mode). Particles at small sizes may be mainly influenced
242 by secondary formation and anthropogenic sources (such as vehicle emissions, coal
243 combustion, industrial emissions, etc.), while particles at large sizes may be more
244 associated with natural sources, resuspended dust (such as road dust, construction dust,
245 mechanical abrasion processes, etc.) and industrial emissions (Hilario et al., 2020). In
246 this work, the peaks in the coarse mode were very strong during spring due to the
247 influences of resuspended dust and natural sources. The enhancement of PM in the fine
248 mode during winter is associated with unfavorable meteorological conditions for the
249 dispersion of fine particles, and increased emissions from coal combustion for heating
250 (Cheng et al., 2016; Tian et al., 2016). The broader peak in the fine mode during winter
251 should be noted.

252 **Figure 1**

253 To explore the causes of heavy pollution, size distributions of PM during the heavy
254 pollution days were compared with less polluted days (all the rest of the days).
255 According to the temporal variations of the size-segregated particle concentrations in
256 Figure S1, most heavy pollution cases occurred in winter and there were only a few
257 days in other seasons. Figure 1 also describes the size distribution of particle mass
258 concentrations for less polluted days and heavy pollution days during four seasons. PM
259 concentrations in the fine mode increased during heavy pollution in all of the seasons.
260 It was also found in several previous studies that fine particles significantly

https://doi.org/10.5194/acp-2020-507
Preprint. Discussion started: 10 August 2020
© Author(s) 2020. CC BY 4.0 License.

Atmospheric Chemistry and Physics Discussions

accumulated during the haze pollution period (Wang et al., 2014; Tian et al., 2016). In spring, the peak in the coarse mode was weaker during heavy pollution than during less polluted days, while the concentrations in the coarse mode significantly increased during summer heavy pollution. Thus, the spring heavy pollution may be associated with sources or processes that engender small particles (like combustion, secondary formation, etc.), while summer heavy pollution was strongly linked with large particle sources (like resuspended dust, dust storms, etc.). During winter and autumn, it is interesting to find that peaks in the fine mode shifted to a larger size, from 0.43-0.65 μm during less polluted days to 0.65-1.1 μm during heavy pollution. This result is consistent with the previous studies, which showed that the peak mass concentration of fine mode particles shifted to larger sizes during heavily polluted days (Tian et al., 2016; Guo et al., 2014). The causes and mechanisms of heavy pollution will be further explored according to the variations of inorganic and organic components.

3.2 Size-resolved chemical compositions and diagnostic ratios

Correlations among size-segregated chemical composition (percentages of 4 ions, 17 elements and 7 carbon fractions accounting for PM concentrations) have been calculated and are summarized in Table S1(a). It is noticeable to find that the compositions were similar in each mode (size<0.43 μm considered as the pseudo-ultrafine mode; 0.43-0.65, 0.65-1.1 and 1.1-2.1 μm as the fine mode; and 2.1-3.3 3.3-4.7, 4.7-5.8, 5.8-9.0 and >9.0 μm in the coarse mode), while they showed relatively high differences between different modes. Additionally, the correlations among size-

https://doi.org/10.5194/acp-2020-507
Preprint. Discussion started: 10 August 2020
© Author(s) 2020. CC BY 4.0 License.

Atmospheric Chemistry and Physics Discussions

segregated composition of organic compounds (percentages of 18 PAHs, 2 cholestane, 7 hopane and 24 n-alkanes accounting for PM concentrations) showed similar trends (Table S1(b)), indicating that both main component composition and organic composition were similar in each mode. Thus, the sizes were aggregated into three modes to investigate the size-segregated compositions: coarse (>2.1 μm), fine (0.43-2.1 μm), and pseudo-ultrafine (< 0.43 μm) modes.

3.2.1 Size-segregated main species

Concentrations of chemical species in the pseudo-ultrafine, fine and coarse modes during the four seasons are shown in Figure 2. The composition of main species were similar during spring, autumn and winter: in the pseudo-ultrafine mode, the primary component was organic carbon fraction OC3 (2.4, 2.0 and 3.2 μg m^{-3} during spring, autumn and winter, respectively); in the fine mode, the primary component was NO_3^- (8.0, 12.7 and 15.1 μg m^{-3}, respectively); and in the coarse mode, the CE (crustal elements, defined as sum of Al, Ca, Fe and Ti) was highest with concentrations of 17.2, 16.0 and 20.2 μg m^{-3}. During summer, the highest components were SO_4^{2-} in the pseudo-ultrafine (1.6 μg m^{-3}) and fine modes (8.2 μg m^{-3}), and CE in the coarse mode (14.8 μg m^{-3}). The sums of OC fractions were higher than other components in most modes and seasons. NO_3^-, SO_4^{2-} and OC are mainly from secondary formation, combustion sources and industrial emissions, and crustal elements are linked with resuspended dust (except during dust storm periods).

The concentration of SO_4^{2-} is the highest among all measured species in the fine mode during summer, while NO_3^- was the primary component during other seasons.

https://doi.org/10.5194/acp-2020-507
Preprint. Discussion started: 10 August 2020
© Author(s) 2020. CC BY 4.0 License.

Atmospheric Chemistry and Physics Discussions

305 During summer, photochemical processes can be more efficient. However, due to the
306 thermodynamic instability of ammonium nitrate, it may decompose under high
307 temperature (Hasheminassab et al., 2014). It is interesting to find that the NO_3^-
308 concentration in the coarse mode was higher during summer (5.7 μg m^{-3}) than during
309 other seasons, which may result from the deposition of nitric acid vapour upon coarse
310 particle surfaces.

311 **Figure 2**

312 **3.2.2 Size-segregated organic compounds and diagnostic ratios**

313 PAHs arise mainly from anthropogenic sources. According to the concentrations of
314 organic compounds in Figure 2, the concentrations of $\sum_{18}$PAHs (summed
315 concentrations of 18 PAHs) were 22, 19, 31 and 49 ng m^{-3} during spring, summer,
316 autumn and winter, respectively. The 5 and 6-ring PAHs (mainly BbF, BeP, BaP, DBA,
317 IPY and BghiP) showed higher concentrations than other PAHs during all four seasons
318 (Figure S2a). High molecular weight PAHs are emitted under a high temperature
319 condition as from vehicles and they are more stable in the particle phase. It is interesting
320 to observe an obvious increase of 4-ring PAHs in the fine mode during winter, which
321 may be caused by coal combustion for residential heating, and the low wintertime
322 temperature favouring partition into the condensed phase. Tianjin is a typical city in
323 northern China with considerable coal burning for house heating during winter, which
324 emits more 4-ring PAHs (Zhang et al., 2017). Moreover, some low-molecular-weight
325 PAHs can be emitted by volatilization and low to moderate temperature combustion,
326 such as during coking (Khalili et al., 1995), biomass combustion (Zhang et al., 2008)

https://doi.org/10.5194/acp-2020-507
Preprint. Discussion started: 10 August 2020
© Author(s) 2020. CC BY 4.0 License.

Atmospheric Chemistry and Physics Discussions

and residential utilization of electricity or gas for heating and cooking (Yadav et al., 2018). Thus, the results suggest that vehicle exhaust, coal combustion, industrial emission and biomass burning had mixed effects on the atmospheric PAH pollution, and that coal burning was one of major sources of PAHs in northern China, especially during winter.

Additionally, diagnostic ratios of organic compounds are may be indicative of sources, so the ratios in size-resolved PM during each season and their ranges for sources are summarized in Table 2. The Ant/(Ant+Phe) ratios were greater than 0.1, confirming an influence from pyrogenic emissions (Han et al., 2018). The IPY/BghiP ranged from 0.66 to 2.51, indicating mixed effects of vehicle emissions and coal combustion (Grimmer et al., 1983). The IPY/BghiP values were lower in the pseudo-ultrafine fraction, implying that vehicle emissions impact was stronger in the pseudo-ultrafine than in other modes. Enhancement of IPY/BghiP ratios during autumn and winter indicates that PAHs derived from coal combustion increased, consistent with the results of 4-ring PAH variations. Due to the low concentrations of organic compounds, the diagnostic ratios are subject to uncertainty, especially for the seasons and modes with lower concentrations.

Table 2

Hopanes and steranes are often used to determine the fuel maturity (Oros and Simoneit, 2000). As shown in Figure 2, the total concentrations of 2 steranes and 7 hopanes ranged from 1 to 5 ng m^{-3} for the pseudo-ultrafine mode, from 4 to 25 ng m^{-3} for fine mode and from 3 to 27 ng m^{-3} for the coarse mode. The maximum occurred in

https://doi.org/10.5194/acp-2020-507
Preprint. Discussion started: 10 August 2020
© Author(s) 2020. CC BY 4.0 License.

Atmospheric Chemistry and Physics Discussions

winter and the minimum occurred in summer. The 17α(H),21β(H)-30-norhopane (C29αβ) and 17α(H),21β(H)-30-hopane (C30αβ) showed the highest levels of the hopanes and steranes during four seasons in all modes, as shown in Figure S2b. The C30αβ mass concentration was higher than C29αβ during spring, summer and autumn, while the contrary occurred during winter. C34αβS and C34αβR concentrations were significantly enhanced during autumn and winter in the fine and coarse modes.

The molecular composition of hopanes are further assessed by their mass ratios. As shown in Table 2, diagnostic ratios of C29αβ/C30αβ indicate a strong traffic influence during summer (C29αβ/C30αβ=0.59-0.69) and a strong coal combustion contribution during winter (ratio=1.32-1.38). The hopane C34[S/(S+R)] ratio, which is an indicator of the maturity of combusted fossil fuel, ranged from 0.27 to 0.75. Hopane [S/(S+R)] ratios increase with increasing fuel maturity. When the level of the R isomer is much higher than the concentration of the S isomer, PM is mainly influenced by emissions from coal combustion, while the similar concentrations of R and S isomer indicate traffic emissions. It was reported that the homohopane index [S/(S+R)] for coal smoke samples increases with coal rank (lignite 0.05; brown coal 0.09; sub-bituminous coal 0.20; bituminous coal 0.35) (Oros and Simoneit, 2000). The C34[S/(S+R)] ratios in this study were more indicative of coal burning during autumn and winter. And we notice that the C34[S/(S+R)] values were generally in the order of pseudo-ultrafine mode > fine mode > coarse mode, indicating that the maturity of the fossil fuel decreased with the increase of particle size. Obvious low values of C34[S/(S+R)] in the coarse mode during winter may indicate an influence of combustion of immature coals.

https://doi.org/10.5194/acp-2020-507
Preprint. Discussion started: 10 August 2020
© Author(s) 2020. CC BY 4.0 License.

Atmospheric Chemistry and Physics Discussions

n-Alkanes are mainly emitted in vehicle emissions, coal combustion, tire-wear particles and particulate abrasion products from leaf epicuticular waxes, and it has been reported that they have unique signatures for different sources (Han et al., 2018). N-alkanes were the most abundant organic compounds, with the total concentrations ranging from 2187 during summer to 4452 ng m^{-3} during winter (Figure 2). As shown in Figure S2 and Table 2, the values of the carbon number of the most abundant n-alkane (Cmax) in this study were C23 in the fine mode and C31 in the coarse mode during spring and summer, and were generally C28 in all modes during autumn and winter. Cmax represents the carbon number of the most abundant n-alkane, which is regarded as an important indicator of biogenic inputs. C23 has been reported as indicative of vehicle emissions (Lyu et al., 2017). C31 mainly comes from a vegetation source (plant wax) and tire-wear source which can be caused by resuspended dust (Han et al., 2018). Thus, the Cmax values in this work suggest a strong fuel combustion influence in the fine mode, and contributions of vegetation sources and resuspended dust in the coarse mode during spring and summer. During autumn and winter, the Cmax=28 was considered to come from local emissions, especially coal combustion (Han et al., 2018).

The CPI (carbon preference index) ranged from 0.73 to 1.48, suggesting a predominant contribution from anthropogenic sources (Han et al., 2018). WNA% and PNA% provide a direct insight that above 75% of n-alkanes were originated from anthropogenic sources. CPI and WNA% consistently demonstrate that n-alkanes were mainly contributed by anthropogenic activities, and the natural source was higher in the

https://doi.org/10.5194/acp-2020-507
Preprint. Discussion started: 10 August 2020
© Author(s) 2020. CC BY 4.0 License.

Atmospheric Chemistry and Physics Discussions

393 coarse mode during spring and summer, consistent with the interpretation of other ratios
394 above.
395
396 **3.3 Seasonality of size distributions**
397 **3.3.1 Size distributions of main components**
398 The size distributions of main chemical species (ions, elements and carbon fractions)
399 during spring, summer, autumn and winter are shown in Figure 3a. NO_3^-, SO_4^{2-} and
400 NH_4^+ mass concentrations were abundant in the fine mode, which exhibited maxima at
401 0.43-0.65 or 0.65-1.1 μm during most seasons, except for SO_4^{2-} in winter (1.1-2.1 μm)
402 and NO_3^- in summer (3.3-4.7 μm). Except for primary sources, the fine mode NO_3^- and
403 SO_4^{2-} can be formed from the gaseous and aqueous phase reactions, and the coarse
404 mode NO_3^- and NH_4^+ can origin from repartitioning and heterogeneous reactions with
405 sea salt and crustal dust (Liu et al., 2017). A strong peak of NO_3^- was observed at 3.3-
406 5.8 μm during summer. Due to the thermodynamic instability, fine mode NH_4NO_3 can
407 be dissociated into vapour at high ambient temperatures and then shifted onto coarse
408 particles by the condensation, reaction, dissolution or coagulation. During spring and
409 summer, the weak peaks of NH_4^+ in the coarse mode may partly derive from suspended
410 soil containing fertilizer. The size distributions of Cl^- showed obvious seasonal
411 variations, which strongly peaked in the fine mode during winter and autumn
412 corresponding to emissions of HCl from combustion sources which can form semi-
413 volatile ammonium chloride (Pio and Harrison, 1987); and peaked in the coarse mode
414 during summer because of sea salt.

https://doi.org/10.5194/acp-2020-507
Preprint. Discussion started: 10 August 2020
© Author(s) 2020. CC BY 4.0 License.

Figure 3

Carbon fractions generally exhibited typical bimodal distributions with peaks in fine and coarse modes. The levels of OC2, OC4 and EC1 in the fine mode and those of OC3 in both fine and coarse modes were significantly enhanced during winter. The OC fractions and EC1 primarily come from coal combustion, vehicle exhaust, and biomass burning, while EC2 and EC3 mainly originate from diesel and oil combustion (Kim and Hopke, 2004; Shi et al., 2016). Thus, the enhancement of these carbon fractions in the fine mode during winter is strongly linked with coal combustion for residential heating. The OC3 in the coarse mode may be influenced by complex emissions and reactions. It has been shown that PM emissions in northern China are complex during winter (Tian et al., 2016), like scattered (area source) coal combustion. Shi et al. (2020) indicated that scattered coal is the largest source of ambient volatile organic compounds during the heating season in Beijing, which are important precursors for secondary organic carbon (SOC). Thus, SOC generation may be another reason for OC enhancement in both fine and coarse modes. Photochemical reactions may be generally weak during winter, but high precursor concentrations, high humidity and high PM concentrations during winter may enhance the aqueous phase and heterogeneous reactions.

The crustal elements (Al, Ca, Fe, Ti, etc.) were primarily concentrated in the coarse mode at 4.7-5.8 or 5.8-9.0 μm. The high wind speed during spring can facilitate the resuspension of dust (such as road dust, soil dust) into the atmosphere and result in the high level of the crustal elements in the coarse mode. K showed a bimodal distribution: the peak in the fine mode may be associated with biomass or coal combustion, and that

https://doi.org/10.5194/acp-2020-507
Preprint. Discussion started: 10 August 2020
© Author(s) 2020. CC BY 4.0 License.

Atmospheric Chemistry and Physics Discussions

in coarse mode associated with natural sources from soil dust and sea salt. Figure S3 shows the ratios between water-soluble ions and corresponding elements in each size. Peaks of K^+/K and Ca^{2+}/Ca were generally in the fine mode, indicating that K and Ca may be contributed by industrial or combustion sources in the fine mode and strongly associated with crustal dust in the coarse mode. A strong peak of Na^+/Na in the coarse mode during summer may indicate impacts of sea salt, consistent in explaining the peak of Cl^- in the coarse mode during summer.

3.3.2 Size distribution of organic markers

Figure 3b describes the size distribution of organic compounds during different seasons. The size distribution varied with seasons and congeners. About 66-79% PAHs were in the pseudo-ultrafine and fine modes, which were higher than the cumulative percentages of hopanes (64-71%) and n-alkanes (56-60%). The sum of 2- and 3-ring PAHs showed a bimodal distribution, while the summed concentrations of 6- and 7-ring PAHs was strongly concentrated in the fine mode. High molecular weight PAHs are less volatile and predominantly formed on smaller particles where they condense immediately after combustion. However, low molecular weight PAHs are more volatile, so they are easily adsorbed on larger particles as the emissions cool down, or can evaporate from the particle-phase into the air and subsequently adsorb/condense onto pre-existing coarser particle (Offenberg and Baker, 1999). The 4- and 5-ring PAHs were found with a unimodal distribution peaking in the fine mode (0.43-1.1 μm) during winter, while they were bimodal during other seasons, due to their repartitioning being enhanced under higher ambient temperatures.

https://doi.org/10.5194/acp-2020-507
Preprint. Discussion started: 10 August 2020
© Author(s) 2020. CC BY 4.0 License.

Atmospheric Chemistry and Physics Discussions

459 Most sterane and hopanes detected in this work were observed with a bimodal
460 distribution. It is interesting to observe the enhancement of 17β(H),21β(H)-hopane
461 (C30ββ) and 17α(H),21β(H)-22R-tetrakishomohopane (C34αβR) in the coarse mode
462 during winter. C30ββ and C34αβR have been regarded as markers of less mature coals,
463 such as lignite and sub-bituminous coal combustion (Oros and Simoneit, 2000). Thus,
464 their increase indicates a contribution from immature coal combustion to coarser PM
465 during winter. For most n-alkanes, a bimodal size distribution was found at 0.43-0.65
466 or 0.65-1.1μm in the fine mode and 3.3-47 or 4.7-5.8 μm in the coarse mode. Total
467 concentrations of C26-C33 showed a strong peak in the coarse mode during spring and
468 summer, indicating a relatively stronger vegetation source and a resuspended dust
469 contribution to PM in the coarse mode.

470 In previous publications, a bimodal distribution of low molecular weight PAHs and
471 a strong peak in the fine mode of high molecular weight PAHs were reported (Lv et al.,
472 2016; Han et al., 2018). The bimodal distribution of most n-alkanes was observed by
473 Wang et al. (2009), Lyu et al. (2017) and Xu et al. (2017). The size distributions of
474 hopanes were reported as unimodal in the fine mode (Kleeman et al., 2008; Han et al.,
475 2018), and can be bimodal during summer (Wang et al., 2009). Through comparing
476 these publications with this work, we find that the size distributions of most organic
477 compounds were consistent, but the peaks in the coarse mode are often stronger in this
478 work. The difference can be due to variations in their sources, increased fine particle
479 coagulation at high particle concentrations, and organic compound repartitioning.
480 Tianjin is an important heavily populated megacity in northern China, which has large

https://doi.org/10.5194/acp-2020-507
Preprint. Discussion started: 10 August 2020
© Author(s) 2020. CC BY 4.0 License.

Atmospheric Chemistry and Physics Discussions

emissions from industry and traffic, and high resuspended dust due to strong human activities (such as construction and heavy trucks activity). The stronger peaks in the coarse mode, especially during spring and summer, may be linked with the high resuspension of dust from coal combustion, industrial emissions, traffic emissions, construction dust, and mechanical abrasion processes.

3.4 Size distributions during less polluted and heavy pollution periods

To explore which sizes and which components are significantly enhanced during heavy pollution periods, the enhancement ratios, which are defined as ratios of component concentration during heavy pollution days to that during other days ($ER_{H/C}=C_H/C_C$), are calculated and shown in Figure 4. There are different formation mechanisms for heavy pollution episodes during different seasons. During spring heavy pollution days, the $ER_{H/C}$ of OC3 and OC4 at 1.1-3.3 μm were significantly high, along with the enhancement of 4- and 5-ring PAHs (Flt, Pry, BbF, BkF, Bap), hopane and C18-C33 at these sizes. Further, Figure 5 compares the size distributions of species which were significantly enhanced during heavy pollution. During the spring heavy pollution, the peaks of the OC3 shifted to 2.1-4.7 μm, and the peaks of 4-ring PAHs, C29αβ-HP, C30αβ-HP and sum of C26-C33 also changed to a larger size. The results imply that this heavy pollution may be caused by local combustion sources which emitted relatively larger particles.

Figure 4

Figure 5

https://doi.org/10.5194/acp-2020-507
Preprint. Discussion started: 10 August 2020
© Author(s) 2020. CC BY 4.0 License.

Atmospheric Chemistry and Physics Discussions

503 The summer heavy pollution was characterized by strong enhancement of SO_4^{2-},
504 NH_4^+, Al, EC2 and C26-33 mainly in the coarse mode (Figure 4). The peak of Al in the
505 coarse mode changed from 4.7-5.8 μm for less/average polluted days to 5.8-9.0 μm for
506 heavy pollution (Figure 5). And SO_4^{2-}, $NH_4^+$and C26-33 increased in size to 3.3-4.7 and
507 5.8-9.0 μm respectively. Consistent with the discussion on size distribution of PM mass
508 concentrations, this heavy pollution may be caused by resuspended dust or long-range
509 transported dust and heterogeneous reactions. Suspended soil containing fertilizer can
510 contribute to alkaline conditions and enhance the heterogeneous reactions on coarse
511 particles (Shen et al., 2011). Additionally, the increases of the low molecular weight
512 PAHs and short chain n-alkanes demonstrate the repartitioning and suspension.

513 Heavy pollution during autumn and winter was strongly associated with significant
514 enhancement of NO_3^- and moderate enhancement of SO_4^{2-}, NH_4^+, OC and EC at most
515 sizes especially at 0.65-3.3 μm, as shown in Figure 4. NO_3^-, SO_4^{2-}, NH_4^+, and OC can
516 be from chemical reactions and partly from primary emissions, while EC is from
517 primary emissions. The enhanced EC demonstrates that the meteorological conditions
518 during heavy pollution caused accumulation of particles and precursors. Referring to
519 Figure 5, peaks of NO_3^-, SO_4^{2-}, OC3 and EC1 in the fine mode shifted from 0.43-0.65
520 μm during less polluted days to 0.65-1.1 or 1.1-2.1 μm during heavy pollution. Heavy
521 pollution during autumn and winter in northern China is usually characterized by large
522 emissions and specific meteorological condition with a stable boundary layer, weak
523 winds, an increase in temperature, and high relative humidity (RH) (Cheng et al., 2016).
524 The meteorological condition was unfavorable for the dispersion of particles and

https://doi.org/10.5194/acp-2020-507
Preprint. Discussion started: 10 August 2020
© Author(s) 2020. CC BY 4.0 License.

Atmospheric Chemistry and Physics Discussions

precursors and favours secondary particle formation, hygroscopic growth and stronger coagulation. Lower temperature, high RH and high precursors increase the formation of ammonium nitrate by facilitating the aqueous phase chemical reactions which was more likely to occur at 0.65-2.1 μm (Zhang et al., 2013; Tian et al., 2016). In addition, as discussed above, the emissions during winter were more complex and emitted coarser EC-containing particles (such as domestic coal combustion), which can rapidly accumulate during heavy pollution conditions. The EC at a coarser size can strength the reaction at these sizes, because EC could provide sites for adsorption and reaction due to its large surface area, and it has the catalytic properties for redox chemistry reactions. Stronger relationship between black carbon (BC)-containing particles and secondary species during more polluted periods were also observed by Wang et al. (2019).

4. Summary and conclusions

A comprehensive study on water-soluble ions, elements, carbon fractions, n-alkanes, PAHs, hopanes and steranes in size-resolved PM samples were conducted during 1 year in a typical northern Chinese industrial megacity. Size distributions of the inorganic and organic components during different seasons and pollution levels were analyzed.

The size distribution of the PM mass concentrations was bimodal during all four seasons peaking at 0.43-0.65 μm and 4.7-5.8 μm; and the coarse mode peak was large during spring and the fine mode peak was more substantial during winter. Both main component composition and organic composition were similar within each mode, but relatively different for the different modes. The OC3, NO_3^- and sum of crustal elements

https://doi.org/10.5194/acp-2020-507
Preprint. Discussion started: 10 August 2020
© Author(s) 2020. CC BY 4.0 License.

Atmospheric Chemistry and Physics Discussions

547 showed the highest concentrations in the pseudo-ultrafine, fine and coarse modes,
548 respectively, except that SO_4^{2-} became the largest component in the pseudo-ultrafine
549 and fine modes during summer. For organic markers, PAHs, C29αβ/C30αβ and
550 C34[S/S+R] ratios consistently indicate stronger traffic influence during summer and
551 increased coal combustion during winter; and imply that the maturity of the fossil fuel
552 source decreased with the increase of particle size. The enhancement of C30ββ and
553 C34αβR in the coarse mode during winter indicate a contribution from immature coal
554 combustion. The profile of *n*-alkanes suggests a dominant fuel combustion influence in
555 the fine mode, and contributions of a vegetation source and resuspended dust in the
556 coarse mode especially during spring and summer.

557 For the size distributions, NO_3^-, SO_4^{2-} and NH_4^+ concentrations were large in the fine
558 mode during most seasons, while SO_4^{2-} peaked at 1.1-2.1 μm during winter probably
559 due to a large contribution of aqueous phase reactions, and NO_3^- peaked at 3.3-4.7 μm
560 during summer due to repartitioning. Carbon fractions generally exhibited typical
561 bimodal distributions. The crustal elements (Al, Ca, Fe, Ti, etc.) were primarily
562 concentrated in the coarse mode at 4.7-5.8 or 5.8-9.0 μm. Most sterane, hopane and n-
563 alkanes were observed to have a bimodal distribution. High molecular weight PAHs
564 were concentrated at small sizes during winter, while low molecular weight PAHs were
565 frequently bimodal due to repartitioning.

566 During the spring heavy pollution periods, OC3, OC4, 4- and 5-ring PAHs, hopane
567 and C18-C33 n-alkanes were enhanced at 1.1-3.3 μm, and their peaks shifted to a larger
568 diameter, implying that the heavy pollution may be caused by a local combustion source

https://doi.org/10.5194/acp-2020-507
Preprint. Discussion started: 10 August 2020
© Author(s) 2020. CC BY 4.0 License.

Atmospheric Chemistry and Physics Discussions

569 which emitted relatively larger particles. During the summer heavy pollution periods,
570 the PM, SO_4^{2-}, NH_4^+, Al, EC and C26-33 concentrations in the coarse mode
571 significantly increased, and their peaks in the coarse mode changed from 3.3-5.8 μm
572 for less polluted days to 5.8-9.0 μm for heavy pollution days, indicating a high
573 contribution of resuspended dust and/or heterogeneous reactions. During winter and
574 autumn, heavy pollution was strongly associated with significant enhancement of NO_3^-
575 and moderate increases for SO_4^{2-}, NH_4^+, OC and EC. Peaks of PM, NO_3^-, SO_4^{2-}, OC3
576 and EC1 in the fine mode shifted from 0.43-0.65 μm during less polluted days to 0.65-
577 1.1 or 1.1-2.1 μm during heavy pollution.
578 The data from this work will be used for quantitative source apportionment, which
579 will be further reported in a subsequent paper.
580
581 **Authors contributions**. YZT designed the research and wrote the draft of the
582 manuscript with contributions from all coauthors. RMH designed and reviewed the
583 manuscript. YCF take part in designing the research. ZBS assisted with data analysis
584 and manuscript edit. YLL, YXL and QQX performed sampling and experiments. JSX
585 assisted with data analysis.
586 **Competing interests.** The authors declare that they have no conflict of interest.
587 **Acknowledgments.** This study is supported by the National Natural Science
588 Foundation of China (21707071), Young Elite Scientists Sponsorship Program by
589 Tianjin, China (TJSQNTJ-2018-04), and China Scholarship Council. RMH, ZS and
590 JSX are supported by Natural Environment Research Council (NE/N007190/1).

https://doi.org/10.5194/acp-2020-507
Preprint. Discussion started: 10 August 2020
© Author(s) 2020. CC BY 4.0 License.

Atmospheric Chemistry and Physics Discussions

591

592 **References**

593 Burnett, R. T., Pope, C. A., Ezzati, M., Olives, C., Lim, S. S., Mehta, S., Shin, H. H.,
594 Singh, G., Hubbell, B., Brauer, M., Anderson, H. R., Smith, K. R., Balmes, J. R.,
595 Bruce, N. G., Kan, H., Laden, F., Prüss-Ustün, A., Turner, M. C., Gapstur, S. M.,
596 Diver, W. R., Cohen, A.: An integrated risk function for estimating the global burden
597 of disease attributable to ambient fine particulate matter exposure, Environ. Health
598 Perspect., 122, 397-403, 2014.

599 Cheng, Y., Zheng, G., Wei, C., Mu, Q., Zheng, B., Wang, Z., Gao, M., Zhang, Q., He,
600 K.B., Carmichael, G., Pöschl, U., and Su, H.: Reactive nitrogen chemistry in aerosol
601 water as a source of sulfate during haze events in China, Sci. Adv., e1601530, 2016.

602 Chow, J. C., Watson, J. G., Pritchett, L. C., Pierson, W. R., Frazier, C. A., and Purcell,
603 R. G.: The DRI thermal/optical reflectance carbon analysis system: Description,
604 evaluation and applications in U.S. air quality studies, Atmos. Environ., 27, 1185-
605 1201, 1993.

606 Dillner, A.M., Schauer, J.J., Zhang, Y., Zeng, L., and Cass, G.R.: Size-resolved
607 particulate matter composition in Beijing during pollution and dust events, J.
608 Geophys. Res., 111, D05203, doi:10.1029/2005JD006400, 2006.

609 Grimmer, G., Jacob, J., and Noujack, K. W.: Profile of the polycyclic aromatic
610 hydrocarbons from lubricating oils, Inventory by GC/MS-PAH in environmental
611 materials, Part 1, Fresen. Z. Anal. Chem., 314, 13-19, 1983.

612 Guo, S., Hu, M., Zamora, M. L., Peng, J., Shang, D., Zheng, J., Du, Z., Wu, Z., Shao,

https://doi.org/10.5194/acp-2020-507
Preprint. Discussion started: 10 August 2020
© Author(s) 2020. CC BY 4.0 License.

Atmospheric Chemistry and Physics Discussions

613 M., Zeng, L., Molina, M. J., and Zhang, R.: Elucidating severe urban haze formation
614 in China, P. Natl. Acad. Sci. USA, 111, 17373-17378, doi:10.1073/pnas.1419604111,
615 2014.
616 Han, D., Fu, Q., Gao, S., Li, L., Ma, Y., Qiao, L., Xu, H., Liang, S., Cheng, P., Chen,
617 X., Zhou, Y., Yu, J. Z., and Cheng, J. P.: Non-polar organic compounds in autumn
618 and winter aerosols in a typical city of eastern China: size distribution and impact of
619 gas-particle partitioning on PM2.5 source apportionment, Atmos. Chem. Phys., 18,
620 9375-9391, 2018.
621 Hasheminassab, S., Daher, N., Saffari, A., Wang, D., Ostro, B. D., Sioutas, C.: Spatial
622 and temporal variability of sources of ambient fine particulate matter (PM2.5) in
623 California, Atmos. Chem. Phys., 12085-12097, 2014.
624 Hilario, M. R. A., Cruz, M. T., Cambaliza, M. O. L., Reid, J. S., Xian, P., Simpas, J. B.,
625 Lagrosas, N. D., Uy, S. N. Y., Cliff, S., and Zhao, Y.: Investigating size-segregated
626 sources of elemental composition of particulate matter in the South China Sea during
627 the 2011 Vasco cruise, Atmos. Chem. Phys., 20, 1255-1276, 2020.
628 Huang, X., Liu, Z., Zhang, J., Wen, T., Ji, D., and Wang, Y.: Seasonal variation and
629 secondary formation of size-segregated aerosol water-soluble inorganic ions during
630 pollution episodes in Beijing, Atmos. Res., 168, 70-79, 2016.
631 Khalili, N.R., Scheff, P.A., Holsen, T.M.: PAH source fingerprints for coke ovens, diesel
632 and gasoline engines, highway tunnels, and wood combustion emissions, Atmos.
633 Environ., 29, 533-542, 1995.
634 Kim, E., and Hopke, P.K.: Improving source identification of fine particles in a rural

https://doi.org/10.5194/acp-2020-507
Preprint. Discussion started: 10 August 2020
© Author(s) 2020. CC BY 4.0 License.

northeastern U.S. area utilizing temperature-resolved carbon fractions, J. Geophys. Res., 109, D09204, doi:10.1029/2003JD004199, 2004.

Kleeman, M. J., Riddle, S. G., and Jakober, C. A.: Size distribution of particle-phase molecular markers during a severe winter pollution episode, Environ. Sci. Technol., 42, 6469-6475, 2008.

Kompalli, S.K., Babu, S.N.S., Satheesh, S.K., Moorthy, K.K., Das, T., Boopathy, R., Liu, D., Darbyshire, E., Allan, J.D., Brooks, J., Flynn, M.J., and Coe, H.: Seasonal contrast in size distributions and mixing state of black carbon and its association with PM1.0 chemical composition from the eastern coast of India, Atmos. Chem. Phys., 20, 3965-3985, 2020.

Liu, S., Wang, C., Zhang, S., Liang, J., Chen, F., and Zhao, K.: Formation and distribution of polycyclic aromatic hydrocarbons (PAHs) derived from coal seam combustion: A case study of the Ulanqab lignite from Inner Mongolia, northern China, Int. J. Coal Geol., 90-91, 126-134, 2012.

Long, X., Tie, X., Zhou, J., Dai, W., Li, X., Feng, T., Li, G., Cao, J., and An, Z.: Impact of the Green Light Program on haze in the North China Plain, China, Atmos. Chem. Phys., 19, 11185-11197, 2019.

Lv, Y., Li, X., Xu, T. T., Cheng, T. T., Yang, X., Chen, J. M., Iinuma, Y., and Herrmann, H.: Size distributions of polycyclic aromatic hydrocarbons in urban atmosphere: sorption mechanism and source contributions to respiratory deposition, Atmos. Chem. Phys., 16, 2971-2983, 2016.

Lyu, Y., Xu, T., Yang, X., Chen, J., Cheng, T., and Li, X.: Seasonal contributions to size-

https://doi.org/10.5194/acp-2020-507
Preprint. Discussion started: 10 August 2020
© Author(s) 2020. CC BY 4.0 License.

resolved n-alkanes (C8-C40) in the Shanghai atmosphere from regional anthropogenic activities and terrestrial plant waxes, Sci. Total Environ., 579, 1918-1928, 2017.

Liu, Z., Xie, Y., Hu, B., Wen, T., Xin, J., Li, X., and Wang, Y.: Size-resolved aerosol water-soluble ions during the summer and winter seasons in Beijing: Formation mechanisms of secondary inorganic aerosols, Chemosphere, 183, 119-131, 2017.

Mastral, A. M., Callen, M., and Murillo, R.: Assessment of PAH emissions as a function of coal combustion variables, Fuel, 75, 1533-1536, 1996.

Offenberg, J. H., and Baker, J. E.: Aerosol size distributions of polycyclic aromatic hydrocarbons in urban and over-water atmospheres, Environ. Sci. Technol., 33, 3324-3331, 1999.

Oros, D.R., and Simoneit, B.R.T.: Identification and emission rates of molecular tracers in coal smoke particulate matter, Fuel, 79, 515-536, 2000.

Pai, S.J., Heald, C.L., Pierce, J.R., Farina, S.C., Marais, E.A., Jimenez, J.L., Campuzano-Jost, P., Nault, B.A., Middlebrook, A.M., Coe, H., Shilling, J.E., Bahreini, R., Dingle, J.H., and Vu, K.: An evaluation of global organic aerosol schemes using airborne observations, Atmos. Chem. Phys., 20, 2637-2665, 2020.

Pio, C.A., and Harrison, R.M.: Vapour pressure of ammonium chloride aerosol: Effect of temperature and humidity, Atmos. Environ., 21, 2711-2715, 1987.

Robinson, A. L., Donahue, N. M., and Rogge, W. F.: Photochemical oxidation and changes in molecular composition of organic aerosol in the regional context, J. Geophy. Res.-Atmos., 111, 375-402, 2006.

https://doi.org/10.5194/acp-2020-507
Preprint. Discussion started: 10 August 2020
© Author(s) 2020. CC BY 4.0 License.

Atmospheric Chemistry and Physics Discussions

679 Rogge, W. F., Hildemann, L. M., Mazurek, M., and Cass, G. R.: Sources of fine organic
680 aerosol, 2. Noncatalyst and catalyst-equipped automobiles and heavy-dutyl diesel
681 trucks, Environ. Sci. Technol., 27, 636-651, 1993.
682 Seinfeld, J. H., and Pandis, S. N.: Atmospheric Chemistry and Physics, John Wiley and
683 Sons, New York, 1998.
684 Shen, J., Liu, X., Zhang, Y., Fangmeier, A., Goulding, K., Zhang, F.: Atmospheric
685 ammonia and particulate ammonium from agricultural sources in the North China
686 Plain, Atmos. Environ., 45, 5033-5041, 2011.
687 Shi, G. L., Peng, X., Liu, J., Tian, Y. Z., Song, D., Yu, H. F., Feng, Y. C., and Russell,
688 A. G.: Quantification of long-term primary and secondary source contributions to
689 carbonaceous aerosols, Environ. Pollut., 219, 897-905, 2016.
690 Tian, S. L., Pan, Y. P., and Wang, Y. S.: Size-resolved source apportionment of
691 particulate matter in urban Beijing during haze and non-haze episodes, Atmos. Chem.
692 Phys., 16, 1-19, 2016.
693 TMSB (Tianjin Municipal Statistics Bureau). Statistic Yearbook of Tianjin 2016. China
694 Statistic Publishing House, Beijing (in Chinese), 2017.
695 Wang, G., Kawamura, K., Xie, M., Hu, S., Gao, S., Cao, J., An, Z., and Wang, Z.: Size-
696 distributions of n-alkanes, PAHs and hopanes and their sources in the urban,
697 mountain and marine atmospheres over East Asia, Atmos. Chem. Phys., 9, 8869-
698 8882, 2009.
699 Wang, J., Liu, D., Ge, X., Wu, Y., Shen, F., Chen, M., Zhao, J., Xie, C., Wang, Q., Xu,
700 W., Zhang, J., Hu, J., Allan, J., Joshi, R., Fu, P., Coe, H., and Sun, Y.: Characterization

https://doi.org/10.5194/acp-2020-507
Preprint. Discussion started: 10 August 2020
© Author(s) 2020. CC BY 4.0 License.

Atmospheric Chemistry and Physics Discussions

of black carbon-containing fine particles in Beijing during wintertime, Atmos. Chem. Phys., 19, 447–458, 2019.

Wang, L. T., Wei, Z., Yang, J., Zhang, Y., Zhang, F. F., Su, J., Meng, C. C., and Zhang, Q.: The 2013 severe haze over southern Hebei, China: model evaluation, source apportionment, and policy implications, Atmos. Chem. Phys., 14, 3151-3173, doi:10.5194/acp-14-3151-2014, 2014.

Wang, Y., Wang, M., Zhang, R., Ghan, S. J., Lin, Y., Hu, J., Pan, B., Levy, M., Jiang, J. H., and Molina, M. J.: Assessing the effects of anthropogenic aerosols on Pacific storm track using a multiscale global climate model, Proc. Natl. Acad. Sci. USA, 111(19), 6894-6899, 2014.

Xu, Q. P., Wang, J. Z., Liu, J. Q., and Peng, S.C.: Particulate Size Distribution and Sources Evaluation of n-Alkanes during Long-Term Haze Episode around Chaohu Lake, Eastern China, Aerosol Air Qual. Res., 17, 1975-1984, 2017.

Xu, S., Ren, L., Lang, Y., Hou, S., Ren, H., Wei, L., Wu, L., Deng, J., Hu, W., Pan, X., Sun, Y., Wang, Z., Su, H., Cheng, Y., and Fu, P.: Molecular markers of biomass burning and primary biological aerosols in urban Beijing: size distribution and seasonal variation, Atmos. Chem. Phys., 20, 3623-3644, 2020.

Yadav, I.C., Devi, N.L., Li, J., Zhang, G.: Polycyclic aromatic hydrocarbons in house dust and surface soil in major urban regions of Nepal: Implication on source apportionment and toxicological effect, Sci. Total Environ., 616-617, 223-235, 2018.

Yao, L., Garmash, O., Bianchi, F., Zheng, J., Yan, C., Kontkanen, J., Junninen, H., Mazon, S.B., Ehn, M., Paasonen, P., Sipilä, M., Wang, M., Wang, X., Xiao, S., Chen,

https://doi.org/10.5194/acp-2020-507
Preprint. Discussion started: 10 August 2020
© Author(s) 2020. CC BY 4.0 License.

Atmospheric Chemistry and Physics Discussions

723 H., Lu, Y., Zhang, B., Wang, D., Fu, Q., Geng, F., Li, L., Wang, H., Qiao, L., Yang,
724 X., Chen, J., Kerminen, V.M., Petäjä, T., Worsnop, D. R., Kulmala, M., and Wang,
725 L.: Atmospheric new particle formation from sulfuric acid and amines in a Chinese
726 megacity, Science, 361, 278 – 281, 2018.
727 Zhang, Y., Dou, H., Chang, B., Wei, Z., Qiu, W., Liu, S., Liu, W., Tao, S.: Emission of
728 polycyclic aromatic hydrocarbons from indoor straw burning and emission inventory
729 updating in China, Ann. N. Y. Acad. Sci. 1140, 218-227, 2008.
730 Zhang, Y., Chen, J., Yang, H., Li, R., Yu, Q.: Seasonal variation and potential source
731 regions of PM 2.5 -bound PAHs in the megacity Beijing, China: impact of regional
732 transport, Environ. Pollut., 231, 329-338, 2017.
733 Zhang, G., Bi, X., Chan, L. Y., Wang, X., Sheng, G., and Fu, J.: Size-segregated
734 chemical characteristics of aerosol during haze in an urban area of the Pearl River
735 Delta region, China, Urban Clim., 4, 74-84, doi:10.1016/j.uclim.2013.05.002, 2013.
736 Zhang, Q., Jiang, X., Tong, D., Davis, S. J., Zhao, H., Geng, G., Feng, T., Zheng, B.,
737 Lu, Z., Streets, D. G., Ni, R., Brauer, M., van Donkelaar, A., Martin, R. V., Huo, H.,
738 Liu, Z., Pan, D., Kan, H., Yan, Y., Lin, J., He, K., and Guan, D.: Transboundary health
739 impacts of transported global air pollution and international trade, Nature, 30, 543,
740 705-709, 2017.
741 Zou, Y., Wang, Y., Zhang, Y., Koo, J.K.: Arctic sea ice, Eurasia snow, and extreme
742 winter haze in China, Sci. Adv., 3, e1602751, 2017.
743

https://doi.org/10.5194/acp-2020-507
Preprint. Discussion started: 10 August 2020
© Author(s) 2020. CC BY 4.0 License.

Atmospheric Chemistry and Physics Discussions

744 **Figure captions**

745

746 **Figure 1** Size distribution of particle mass concentrations during spring, summer,
747 autumn and winter for seasonal average, less polluted samples and heavy pollution
748 samples (with PM concentrations higher than the 3rd quartile).

749 **Figure 2** Concentrations of chemical species in the pseudo-ultrafine mode (size<0.43
750 μm), fine mode (0.43-2.1μm) and coarse mode (>2.1μm) during four seasons.
751 CE is crustal elements, defined as sum of Al, Ca, Fe and Ti.
752 Full names and abbreviations of organic compounds are listed in Table 1.

753 **Figure 3 a** Size distribution of main species during spring, summer, autumn and winter.
754 **b** Size distribution of organic compounds during spring, summer, autumn and winter.

755 **Figure 4** Concentration enhancement ratios (which is defined as ratios of component
756 concentration during heavy pollution days to that during less polluted days,
757 $ER_{H/C}=C_H/C_C$) of main species and organic compounds in each size during four seasons.

758 **Figure 5** Size distribution of main species during heavy pollution and less polluted days
759 for spring, summer, autumn and winter.

760

761

762

https://doi.org/10.5194/acp-2020-507
Preprint. Discussion started: 10 August 2020
© Author(s) 2020. CC BY 4.0 License.

Atmospheric Chemistry and Physics Discussions

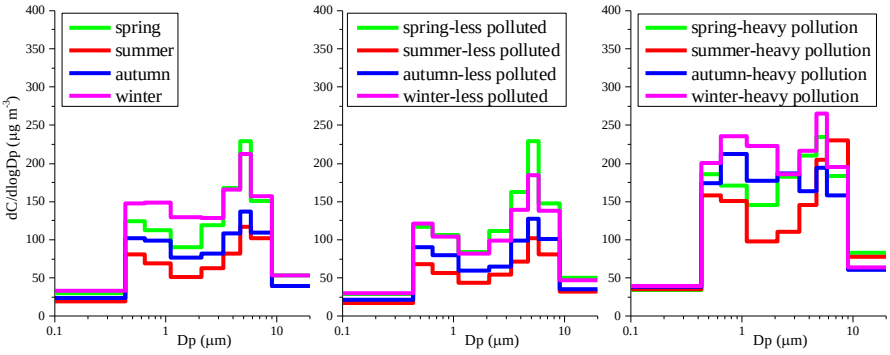

Figure 1 Size distribution of particle mass concentrations during spring, summer, autumn and winter for seasonal average, less polluted samples and heavy pollution samples (with PM concentrations higher than the 3rd quartile).

https://doi.org/10.5194/acp-2020-507
Preprint. Discussion started: 10 August 2020
© Author(s) 2020. CC BY 4.0 License.

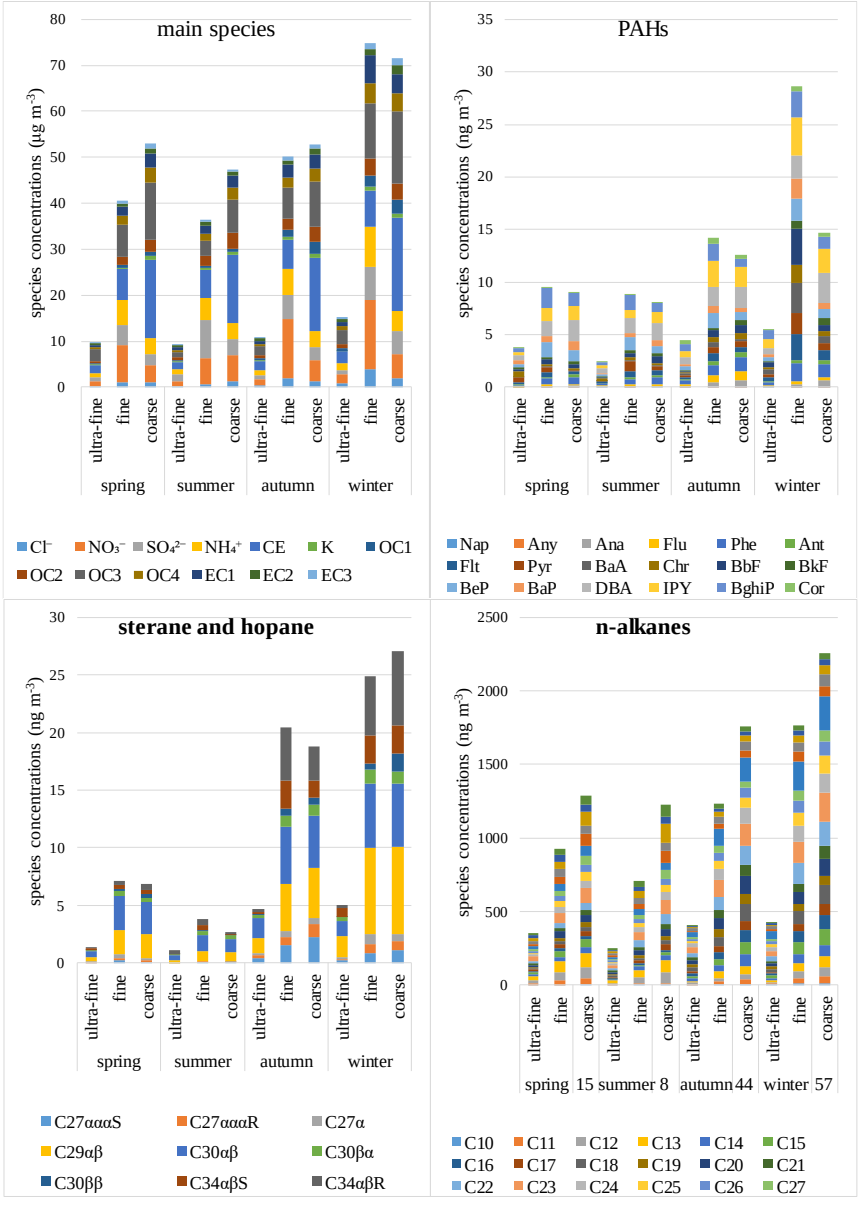

Figure 2 Concentrations of chemical species in the pseudo-ultrafine mode (size<0.43 μm), fine mode (0.43-2.1μm) and coarse mode (>2.1μm) during four seasons. CE is crustal elements, defined as sum of Al, Ca, Fe and Ti. Full names and abbreviations of organic compounds are listed in Table 1.

https://doi.org/10.5194/acp-2020-507
Preprint. Discussion started: 10 August 2020
© Author(s) 2020. CC BY 4.0 License.

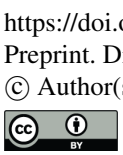

Atmospheric Chemistry and Physics Discussions

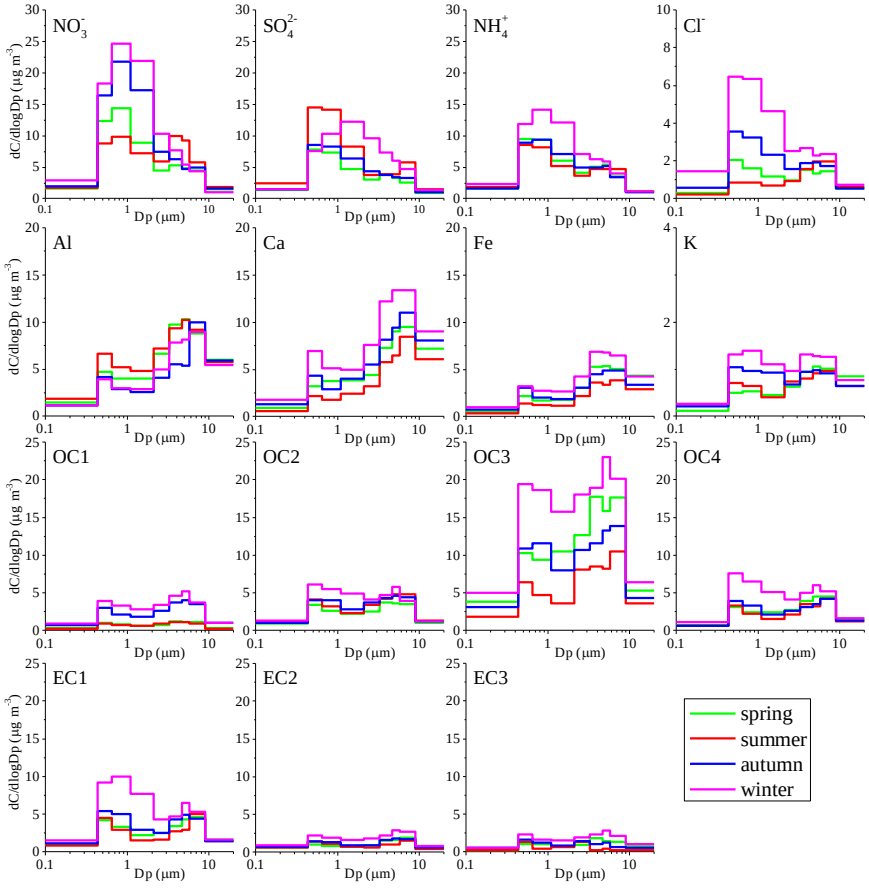

774

775 **Figure 3a** Size distribution of main species during spring, summer, autumn and winter.

https://doi.org/10.5194/acp-2020-507
Preprint. Discussion started: 10 August 2020
© Author(s) 2020. CC BY 4.0 License.

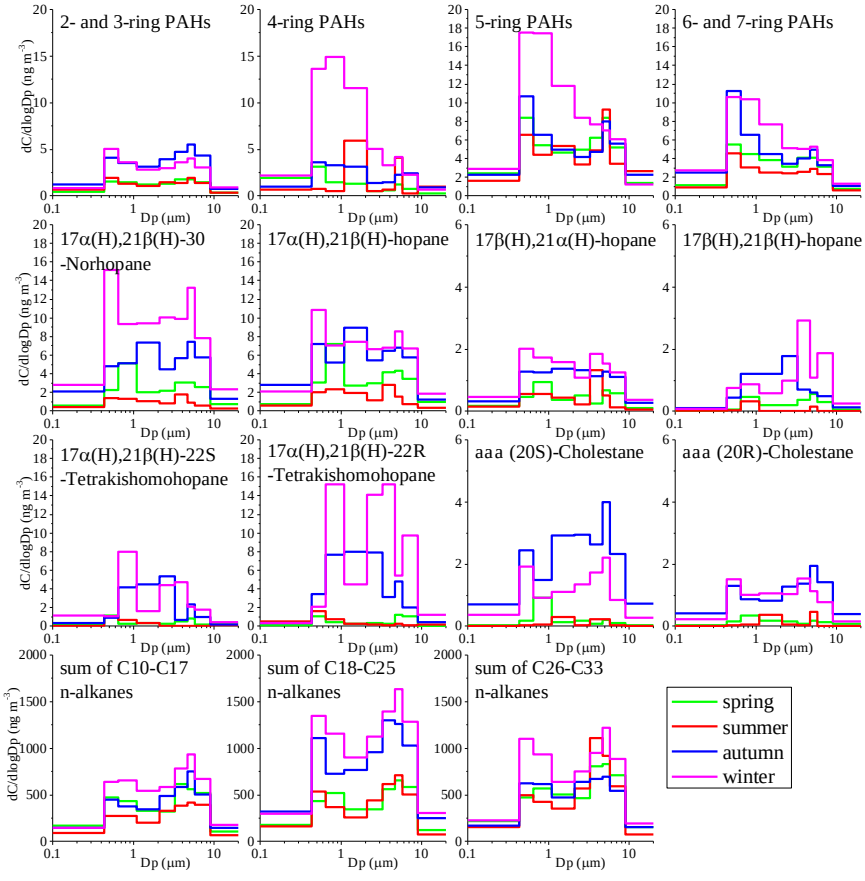

Figure 3b Size distribution of organic compounds during spring, summer, autumn and winter.

https://doi.org/10.5194/acp-2020-507
Preprint. Discussion started: 10 August 2020
© Author(s) 2020. CC BY 4.0 License.

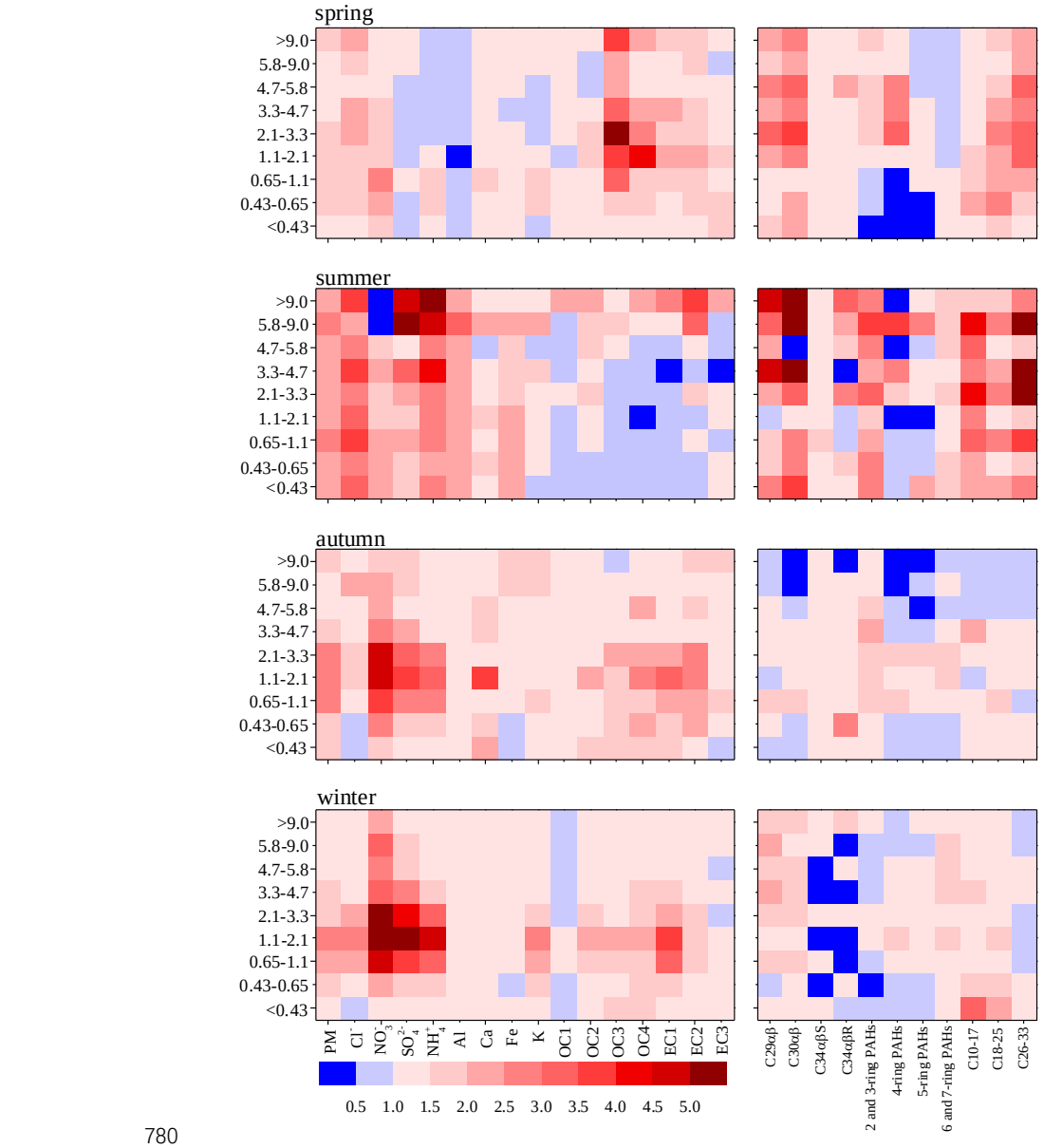

Figure 4 Concentration enhancement ratios (which is defined as ratios of component concentration during heavy pollution days to that during less polluted days, $ER_{H/C}=C_H/C_C$) of main species and organic compounds in each size during four seasons.

https://doi.org/10.5194/acp-2020-507
Preprint. Discussion started: 10 August 2020
© Author(s) 2020. CC BY 4.0 License.

Atmospheric Chemistry and Physics Discussions

785

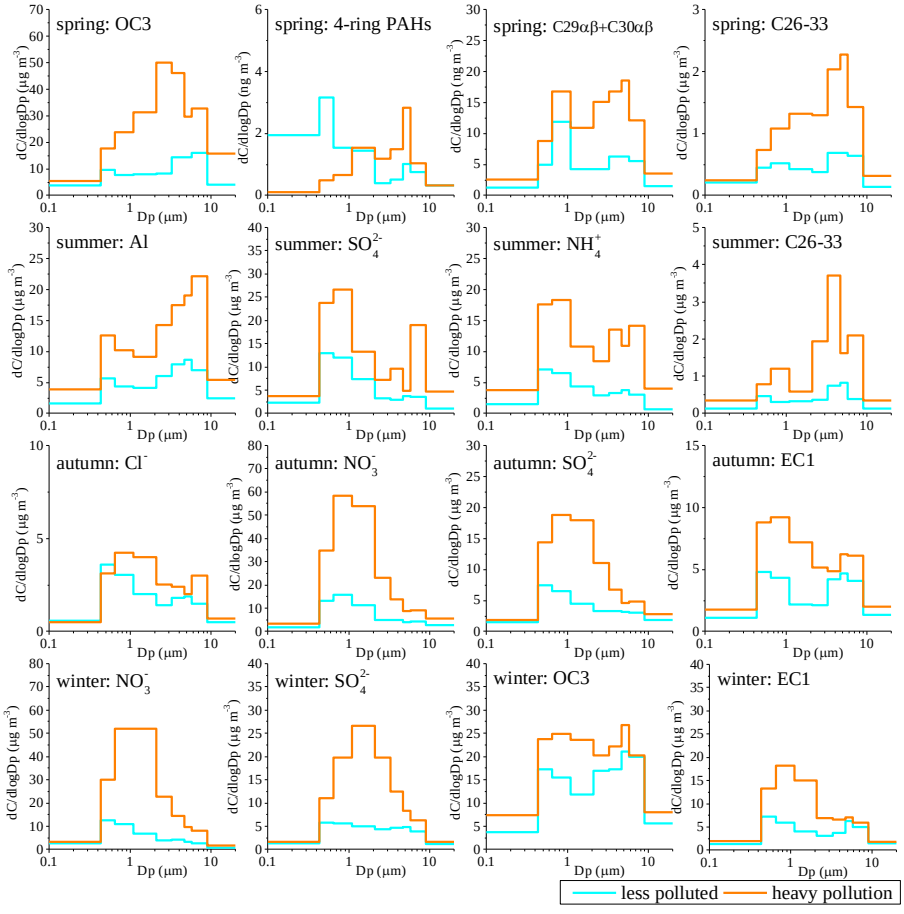

786

787 **Figure 5** Size distribution of main species during heavy pollution and less polluted days
788 for spring, summer, autumn and winter.

789

https://doi.org/10.5194/acp-2020-507
Preprint. Discussion started: 10 August 2020
© Author(s) 2020. CC BY 4.0 License.

Atmospheric Chemistry and Physics Discussions

790 **Table 1** Full names and abbreviations of organic compounds.

Full name	Abbreviation	Full name	Abbreviation
PAHs		**n-alkanes**	
Naphthalene	Nap	n-Decane	C10
Acenaphthylene	Any	Undecane	C11
Acenaphthene	Ana	Dodecane	C12
Fluorene	Flu	Dridecane	C13
Phenanthrene	Phe	Tetradecane	C14
Anthracene	Ant	Pentadecane	C15
Fluoranthene	Flt	Hexadecane	C16
Pyrene	Pyr	Heptadecane	C17
Benz[a]anthracene	BaA	Octadecane	C18
Chrysene	Chr	Nonadecane	C19
benzo[b]fluoranthene	BbF	Icosane	C20
Benzo[k]fluoranthene	BkF	Henicosane	C21
Benzo[e]pyrene	BeP	Docosane	C22
Benzo[a]pyrene	BaP	Tricosane	C23
Dibenzo[a,h]anthracene	DBA	Tetracosane	C24
Indeo[1,2,3-cd]pyrene	IPY	Pentacosane	C25
Benzo[g,h,i]perylene	BghiP	Hexacosane	C26
Coronene	Cor	Heptacosane	C27
Sterane and hopane		Octacosane	C28
ααα (20S)-Cholestane	C27αααS	Nonacosane	C29
ααα(20R)-Cholestane	C27αααR	Triacontane	C30
17a(H)-22,29,30-Trisnorhopane	C27α	Hentriacontane	C31
17α(H),21β(H)-30-Norhopane	C29αβ	Dotriacontane	C32
17α(H),21β(H)-hopane	C30αβ	Tritriacontane	C33
17β(H),21α(H)-hopane	C30βα		
17β(H),21β(H)-hopane	C30ββ		
17α(H),21β(H)-22S-Tetrakishomohopane	C34αβS		
17α(H),21β(H)-22R-Tetrakishomohopane	C34αβR		

791

https://doi.org/10.5194/acp-2020-507
Preprint. Discussion started: 10 August 2020
© Author(s) 2020. CC BY 4.0 License.

Atmospheric Chemistry and Physics Discussions

792 **Table 2** Diagnostic parameters and isomeric ratios of organic compounds in size-resolved PM during each season.

spring	Ant/(Ant+Phe)	IPY/BghiP	C29αβ/C30αβ	C34[S/(S+R)]	Cmax	CPI	WNA%	PNA%
ultra	0.24	0.70	0.78	0.62	C23	1.33	19%	81%
fine	0.22	0.67	0.73	0.51	C23	1.22	18%	82%
coarse	0.23	1.09	0.74	0.63	C31	1.64	24%	76%
summer								
ultra	0.23	0.64	0.69	0.49	C23	0.97	18%	82%
fine	0.27	0.57	0.59	0.41	C23	1.10	17%	83%
coarse	0.28	1.17	0.68	0.35	C31	1.41	24%	76%
autumn								
ultra	0.27	0.75	0.73	0.48	C23	0.81	18%	82%
fine	0.25	1.64	0.82	0.33	C28	0.86	18%	82%
coarse	0.23	2.51	0.97	0.35	C28	0.78	18%	82%
winter								
ultra	0.24	0.87	1.32	0.75	C28	0.76	18%	82%
fine	0.15	1.53	1.33	0.33	C28	0.83	14%	86%
coarse	0.24	1.92	1.38	0.25	C28	0.86	16%	84%
values in references	> 0.1 for pyrogenic sources [a]	0.2, 0.5 and 1.3 for gasoline, diesel and coal combustions [b]	0.6-0.7 for gasoline, 0.4 for diesel [c], 0.6-2.0 for coal [d]	0.05-0.35.for coal, larger for vehicles [d]	C31 for resuspended dust, C23 for vehicle	CPI < 2 petrogenic sources		

793 a Han et al., 2018
794 b Grimmer et al., 1983
795 c Rogge et al., 1993
796 d Oros and Simoneit, 2000

797